Uropod elongation is a common final step in leukocyte extravasation through inflamed vessels

Young-Min Hyun,[1] Ronen Sumagin,[2] Pranita P. Sarangi,[1] Elena Lomakina,[3] Michael G. Overstreet,[1] Christina M. Baker,[1] Deborah J. Fowell,[1] Richard E. Waugh,[3] Ingrid H. Sarelius,[2] and Minsoo Kim[1]

[1]Department of Microbiology and Immunology, David H. Smith Center for Vaccine Biology and Immunology; [2]Department of Pharmacology and Physiology; and [3]Department of Biomedical Engineering, University of Rochester, Rochester, NY 14642

The efficient trafficking of immune cells into peripheral nonlymphoid tissues is key to enact their protective functions. Despite considerable advances in our understanding of cell migration in secondary lymphoid organs, real-time leukocyte recruitment into inflamed tissues is not well characterized. The conventional multistep paradigm of leukocyte extravasation depends on CD18 integrin–mediated events such as rapid arrest and crawling on the surface of the endothelium and transmigration through the endothelial layer. Using enhanced three-dimensional detection of fluorescent CD18 fusion proteins in a newly developed knockin mouse, we report that extravasating leukocytes (neutrophils, monocytes, and T cells) show delayed uropod detachment and become extremely elongated before complete transmigration across the endothelium. Additionally, these cells deposit CD18$^+$ microparticles at the subendothelial layer before retracting the stretched uropod. Experiments with knockout mice and blocking antibodies reveal that the uropod elongation and microparticle formation are the result of LFA-1–mediated adhesion and VLA-3–mediated cell migration through the vascular basement membrane. These findings suggest that uropod elongation is a final step in the leukocyte extravasation cascade, which may be important for precise regulation of leukocyte recruitment into inflamed tissues.

CORRESPONDENCE
Minsoo Kim:
minsoo_kim@urmc.rochester.edu

Abbreviations used: EM, electron microscopy; HUVEC, human umbilical vein endothelial cell; KI, knockin; LysM, lysozyme M; mCFP, monomeric CFP; MP-IVM, multiphoton intravital microscopy; TEM, transendothelial migration.

The maintenance of homeostatic immune surveillance and the development of protective immune responses require that leukocytes efficiently cross tissue barriers and traffic throughout the body, moving in and out of the bone marrow and through lymphoid and nonlymphoid tissues under both normal and infected or inflamed conditions (von Andrian and Mackay, 2000). The conventional multistep paradigm in leukocyte extravasation consists of a cascade of events, including tethering and rolling interactions of leukocytes on the endothelial surface (step 1), leukocyte activation by the local chemokines and/or other inflammatory signals resulting in the activation of integrin adhesiveness (step 2), and the firm adhesion of leukocytes to the blood vessel wall (step 3). The entire process is then followed by crawling and transendothelial migration (TEM), by which leukocytes leave the blood stream and enter the site of inflammation (Nourshargh et al., 2010). The CD18 integrins (also known as β_2 integrins), which include LFA-1 (CD11a/CD18) and Mac-1 (CD11b/CD18), are central components of this process. The CD18 integrins are expressed on the surface of most leukocytes and play a major role in regulating leukocyte adhesion and recruitment to damaged or infected tissues during inflammation.

Although leukocyte recruitment is key for the host defense against infection and injury, the deregulation and/or massive infiltration of active leukocytes could damage the vasculature and underlying tissues. Indeed, leukocyte–endothelial interactions and cell emigration are crucial events that lead to plasma leakage and organ dysfunction. However, studies using in vivo (Zeng et al., 2002) and in vitro (Huang et al., 1988; Burns et al., 1997) models have

The Rockefeller University Press $30.00
J. Exp. Med. 2012 Vol. 209 No. 7 1349-1362
www.jem.org/cgi/doi/10.1084/jem.20111426

The Journal of Experimental Medicine

suggested that little change occurs in vessel and endothelial cell barrier function during the transmigration of leukocytes. These studies suggest the presence of mechanisms that uncouple leukocyte transmigration from endothelial barrier function for macromolecular transport (He, 2010). Endothelial cells form a transmigratory cup, which is a membrane projection enriched with ICAM-1 and VCAM-1 that surrounds adherent leukocytes on the apical side of the endothelium (Carman and Springer, 2004). Emigrating leukocytes are then encapsulated in endothelial domes to minimize increases in vascular permeability (Phillipson et al., 2008). During the procedure, leukocyte LFA-1 and endothelial ICAM-1 remain bound and are redistributed together to form a distinct ring-like structure, which is maintained until TEM is complete (Shaw et al., 2004). After TEM and before approaching the interstitial area, leukocytes must detach their tails from the basolateral side of the endothelial layer and/or basement membrane. Thus, leukocyte tail detachment is considered to be a final step in the completion of leukocyte extravasation, although it is not clear how this event occurs.

The functions of the CD18 integrins have been studied using monoclonal antibodies and small-molecule inhibitors that block integrin-mediated adhesion as well as gene-deficient mice that do not express integrins or their ligands. Given the importance of the dynamic regulation of integrin activation during leukocyte migration, simple loss-of-function approaches are not sufficient to gain an understanding of integrin biology in vivo. Despite recent advances in studies concerning leukocyte migration and trafficking in lymphoid and nonlymphoid tissues, the visualization of endogenous cell surface molecules on intact tissues has been challenging (Bonasio et al., 2007; Friedman et al., 2010). In this study, we generated a knockin (KI) mouse in which CD18 is fused with monomeric CFP (mCFP). With enhanced three-dimensional detection and extended in vivo z-series sections using multiphoton intravital microscopy (MP-IVM), we report that extravasating leukocytes (neutrophils, monocytes, and effector T cells) at the tissue site show delayed uropod detachment and become extremely elongated before the completion of transmigration across the endothelium. Surprisingly, these cells deposit $CD18^+$ microparticles at the subendothelial layer while retracting the stretched uropod.

RESULTS

Generation of KI mice in which CD18 is fused with mCFP

Live cell imaging of fluorescent cell membrane fusion proteins, including a recent approach to visualize LFA-1 on the surface of live T cells using a genetically encoded tag that binds to quantum dot (Bonasio et al., 2007), has been limited to in vitro assays and mostly transparent organisms in vivo. To visualize the real-time subcellular distribution of endogenous CD18 during leukocyte migration in intact tissues, we generated a KI mouse in which CD18 is fused with mCFP (Fig. 1 A). CD18-mCFP mice are fertile and exhibit no obvious phenotypical or functional abnormalities. The correct integration of the mutant CD18 gene into the mouse germline (Fig. 1 A) was confirmed using Southern blot and PCR for WT, heterozygous (+/−), and homozygous (+/+) mice (Fig. 1, B and C). Spleen lysates were subjected to Western blot analysis, and the CD18-mCFP was detected using an anti-GFP antibody, which cross-reacts with CFP (Fig. 1 D). No evidence of the proteolytic cleavage of CFP was detected in heterozygous and homozygous mice (Fig. 1 D). Western blot analysis using anti–mouse CD18 showed an increase in the molecular weight of CD18-mCFP corresponding to the size of mCFP compared with WT CD18 (Fig. 1 D). The total protein (confirmed by Western blot) and cell surface (confirmed by flow cytometry) expression levels of CD18 in WT and CD18-mCFP homozygous mice were similar (Fig. 1, D and E). In heterozygous mice, however, we generally detected more WT CD18 molecules than CD18-mCFP in Western blot analysis (Fig. 1 D), even though the total cell surface expression level of CD18 was identical to the expression level in WT mice. In this study, we used only CD18-mCFP homozygous mice to corroborate our findings. The majority of CD18-mCFP expressed in splenocytes from homozygous mice was evenly distributed at the plasma membrane (Fig. 1 F). We further confirmed that CD18 expression levels in neutrophils, monocytes, and T cells from CD18-mCFP mice were similar to those in WT mice (Fig. 1 G). Naive CD4 T cells from WT and CD18-mCFP mice showed similar migration velocities, displacements, and meandering index on ICAM-1– and CCL21–coated surfaces (Fig. 1 H). We also examined whether the KI animal is more susceptible to infection because of abnormalities in the immune response. No significant defects in bacterial clearance were observed in the peritoneal lavage at 6 and 24 h after septic challenge with cecal ligation and puncture (Fig. 1 I; Rittirsch et al., 2009). A key prerequisite for our experiments is to verify that our CD18-mCFP mice exhibit the normal migratory properties of leukocytes in vivo. Intravital imaging of the leukocytes in the venules of the TNF-treated cremaster muscle revealed that the number of adherent leukocytes and the velocity of the rolling leukocytes in CD18-mCFP mice were not different than those in WT mice (not depicted).

Uropod elongation is a common final step in leukocyte extravasation

Transgenic mice used in MP-IVM express fluorescence probes intracellularly, thus allowing the visualization of cellular positioning or cell–cell interactions; however, the fluorescence signal in our CD18-mCFP KI mouse was predominantly localized at the cell membrane (Fig. 1 F). With this mouse, we performed optimal scanning of leukocyte morphology to detect novel cellular structures during cell migration. Live MP-IVM images showed that leukocyte adhesion increased significantly in the blood vessels in response to CXCL2 superfusion (Phillipson et al., 2006), and a large number of $CD18^+$ cells actively emigrated from the cremaster venules (Fig. 2 A and Video 1). Strikingly, MP-IVM revealed that the majority of extravasating leukocytes were extremely elongated during transmigration (Fig. 2 B and Video 1). The elongated leukocytes

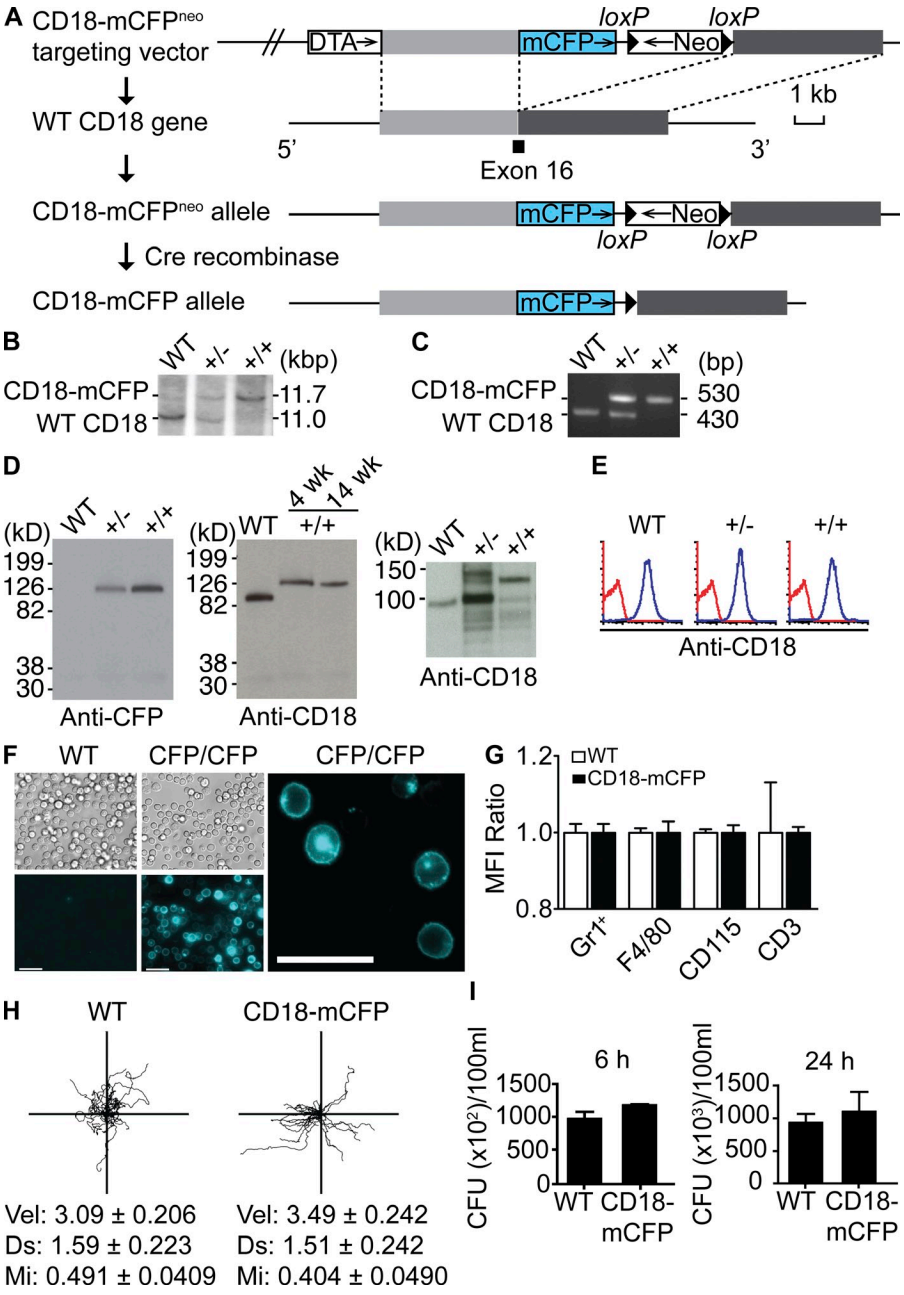

Figure 1. Generation of CD18-mCFP KI mice. (A) Gene targeting procedure for CD18-mCFP KI mice. The mCFP sequence was knocked into the C terminus of the mouse integrin CD18 subunit. (B and C) Southern blot (B) and PCR (C) analyses were performed using genomic DNA isolated from the tails of WT, CD18-mCFP heterozygous (+/−), and homozygous (+/+) mice. (D) Western blot analyses for both CFP and CD18 were performed using spleen lysates from WT, heterozygous, and homozygous mice. For the Western blot analysis of CD18 integrin, WT mice and two homozygous mice with different ages (4 and 14 wk old) were used. A representative image is shown from experiments repeated three times. (E) The cell surface expression of CD18 was measured on neutrophils isolated from WT, heterozygous, and homozygous mice (blue; red, isotype control) by flow cytometry. A representative dataset is shown from experiments repeated three times. (F) The CD18-mCFP expression in splenocytes isolated from homozygous mice was visualized. Bars, 20 µm. (G) Granulocytes (Gr1+), macrophages (F4/80), monocytes (CD115), and T cells (CD3) were isolated from WT and CD18-mCFP mice, labeled with anti-CD18 antibody, and analyzed by flow cytometry to compare the cell surface expression of CD18. MFI, mean fluorescence intensity. (H) In vitro migration of naive CD4 T cells isolated from CD18-mCFP and WT mice was performed on ICAM-1– and CCL21-coated surfaces at 37°C. The cell migration velocity (Vel; µm/min), displacement rate (Ds; µm/min), and meandering index (Mi; µm/µm) shown in the figure were not significantly different. A dataset represents data from experiments repeated three times. (I) The local bacterial burden of WT and CD18-mCFP mice was evaluated at 6 and 24 h in the peritoneal lavage after sepsis challenge by cecal ligation and puncture. (G and I) Representative datasets are shown from experiments repeated three times. The results are expressed as the mean ± SEM.

reached >30 µm in length, which is at least fourfold longer than the size of the rolling and crawling leukocytes in the blood vessel. Additionally, >50% of the total leukocytes spent >20 min before detaching the uropod from the subendothelium and proceeding into the interstitium in response to CXCL2, fMLP, and TNF (Fig. 2, A–E; and Video 1). A linear regression analysis showed a significant positive correlation of the maximum cell length with the extravascular retention time, suggesting that leukocyte extravasation becomes delayed because of tail elongation (Fig. 2 F).

CD18 is expressed on all leukocyte subsets; therefore, we closely examined uropod elongation during cell extravasation on individual cell types using mouse strains with differentiated leukocyte classes. Neutrophils were visualized in WT mice through the i.v. injection of low doses of the Alexa Fluor 488–anti-Gr1 antibody (Chiang et al., 2007). We also conducted in vivo imaging in lysozyme M (LysM)–GFP mice, in which neutrophils and monocytes were labeled with GFP (Faust et al., 2000), and in CX_3CR1-GFP mice, which express GFP in monocytes, natural killer cells, and some T cells (Jung et al., 2000). Finally, the morphology of extravasating effector CD4 T cells was analyzed after the adoptive transfer of the CFSE-labeled cells into WT recipient mice. After the venules were stimulated with chemokines or fMLP, we found that uropod elongation in all leukocyte subsets was similar to that observed in CD18-mCFP mice (Fig. 3, A and B; and Videos 2–5).

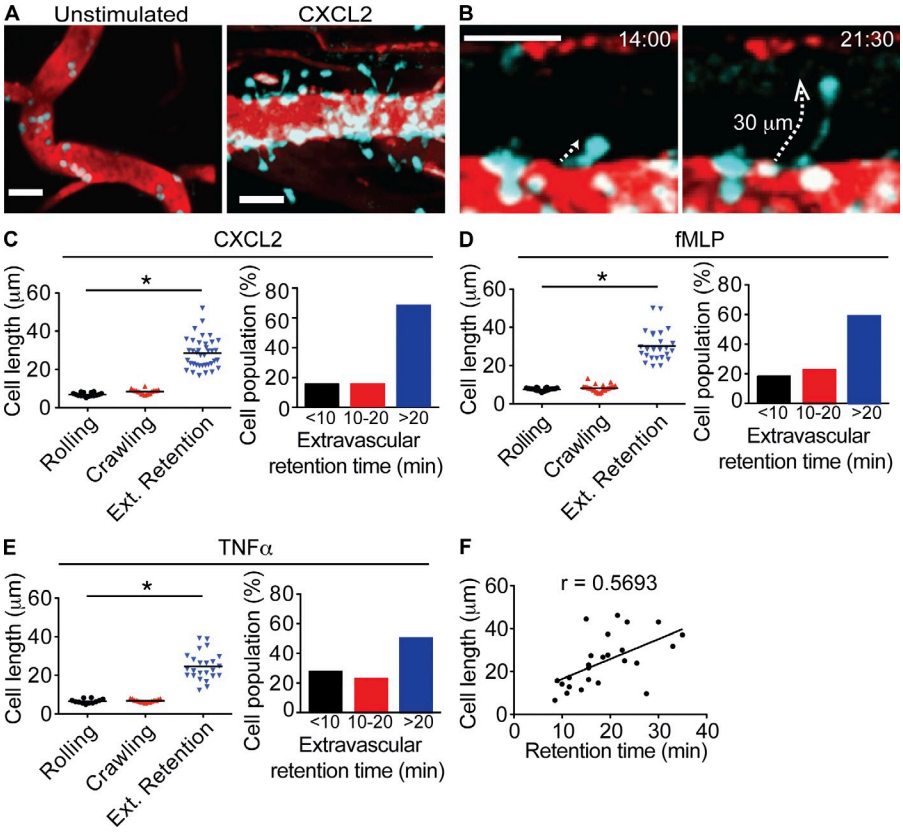

Figure 2. Uropod elongation during leukocyte extravasation of CD18-mCFP mice. (A) CD18-mCFP mice were used to visualize leukocytes in cremaster venules using MP-IVM. The rolling leukocytes were visualized in the unstimulated cremaster muscle venules (left). The venules were stimulated with chemokine (1 nM CXCL2), and the adhered/extravasating leukocytes are shown (right). Texas red dextran was i.v. injected to stain the blood vessel (red). A representative still image is shown from at least 10 stimulated venule images from the cremasters of five mice. See corresponding Video 1. (B) Representative time-lapse images of cell elongation during leukocyte extravasation were taken from the videos of CXCL2-stimulated venules in CD18-mCFP mice. The arrows indicate the elongation direction. Bars, 30 μm. (C–E) Cell lengths in each step of transmigration, rolling, crawling, and extravascular (Ext.) retention. The extravascular retention times were also measured in CXCL2 (C)-, fMLP (D)-, and TNF (E)-stimulated cremaster venules of CD18-mCFP mice. The cell lengths were determined from the longest distance across cells (from head to tail) at each stage. The extravascular retention times represent the time period between the end of TEM and the completion of tail detachment from the endothelium. The cell length and the extravascular retention time were measured from images of at least three venules stimulated for >30 min. Horizontal lines indicate the mean. *, $P < 0.005$. (F) Correlation between the elongation and the extravascular retention time during leukocyte extravasation. The cell length and the extravascular retention time were measured from images of at least three venules stimulated for >30 min with CXCL2. $P = 0.003$.

To further evaluate leukocyte elongation in the endothelia of different tissues during infection, we next investigated the extravasation of LysM-GFP cells in *Candida albicans*– or *Leishmania major*–infected mouse ears. Similar to the cells in the cremaster venules, extravasating LysM-GFP cells in the infected ear venules also exhibited extreme uropod elongation (Fig. 3 C and Video 6). Therefore, our data suggest that uropod elongation is a common final step of leukocyte extravasation.

Elongation is mediated by LFA-1 at the tail of extravasating leukocytes

To analyze the ultrastructure of leukocyte tail elongation, we first performed scanning electron microscopy (EM). We found that the elongated leukocytes were located at the perivascular area, whereas the tip of the uropod remained tethered within the basement membrane (Fig. 4 A). Transmission EM further revealed that the tip of the uropod was not located inside the lumen of the vessel or on the apical side of the endothelial cells; instead, the tip was always attached to the basolateral side of the endothelial cell layer (Fig. 4 B). These data suggest that uropod elongation results from the strong interaction between the tail of the extravasating leukocytes and the basolateral membrane of the endothelial cell layer. The strong adhesive interaction between the leukocytes and the endothelium is largely mediated through interactions between the CD18 integrins (LFA-1 and Mac-1) and ICAM-1 (Sarantos et al., 2008; Bartholomäus et al., 2009; Sumagin et al., 2010). This bond at the leukocyte uropod must be released once TEM is complete, allowing the migration of the leukocytes into the interstitium. Fluorescence microscopy of extravasating leukocytes revealed that CD18 was localized at the leukocyte uropod (Fig. 4 C). Although the uropodal distribution of CD18-mCFP signals during leukocyte extravasation indicated a possible role for CD18 in the interaction between the uropod of extravasating leukocytes and the basolateral membrane of the endothelial cell layer, it was unclear whether a direct relationship existed between CD18 and uropod elongation. To explore this potential relationship, we i.v. injected LFA-1 and Mac-1 blocking antibodies that readily diffuse into the subendothelial layer (Fig. 4 D), where they could inhibit specific CD18 integrins that mediate stable and prolonged tail retention during uropod elongation. The i.v. injection of a Mac-1 (CD11b) blocking antibody resulted in the rapid detachment of intravascular adherent cells during CXCL2 stimulation, whereas the cell length and elongation time were not affected in the extravascular area (Fig. 4, E and F; and Video 7). The i.v. injection of an LFA-1 (CD11a) blocking antibody also resulted in the clearance of adherent intravascular cells,

but, in contrast to the Mac-1 blocking antibody, the uropod length of extravascular leukocytes was significantly decreased, and the majority of leukocytes detached their uropods quickly from the endothelium, spending <10 min in attachment compared with the control IgG–injected mice (Fig. 4, E and F; and Video 8). To further evaluate the specific role of LFA-1 in the uropod elongation, we used CD11a KO mice. Although few CD11a-deficient leukocytes were adhered after CXCL2 stimulation, those cells that could complete TEM showed no significant uropod elongation and detached from the endothelium more quickly than WT cells (Fig. 4, G and H; and Video 9). Importantly, blocking LFA-1 and Mac-1 did not significantly affect the cell migration velocity in the tissue interstitium (Fig. 4 I).

VLA-3 mediates penetration through the basement membrane

The process of leukocyte migration involves at least three interdependent events: attachment at the leading edge, cell contraction, and detachment at the trailing edge. Therefore, leukocyte

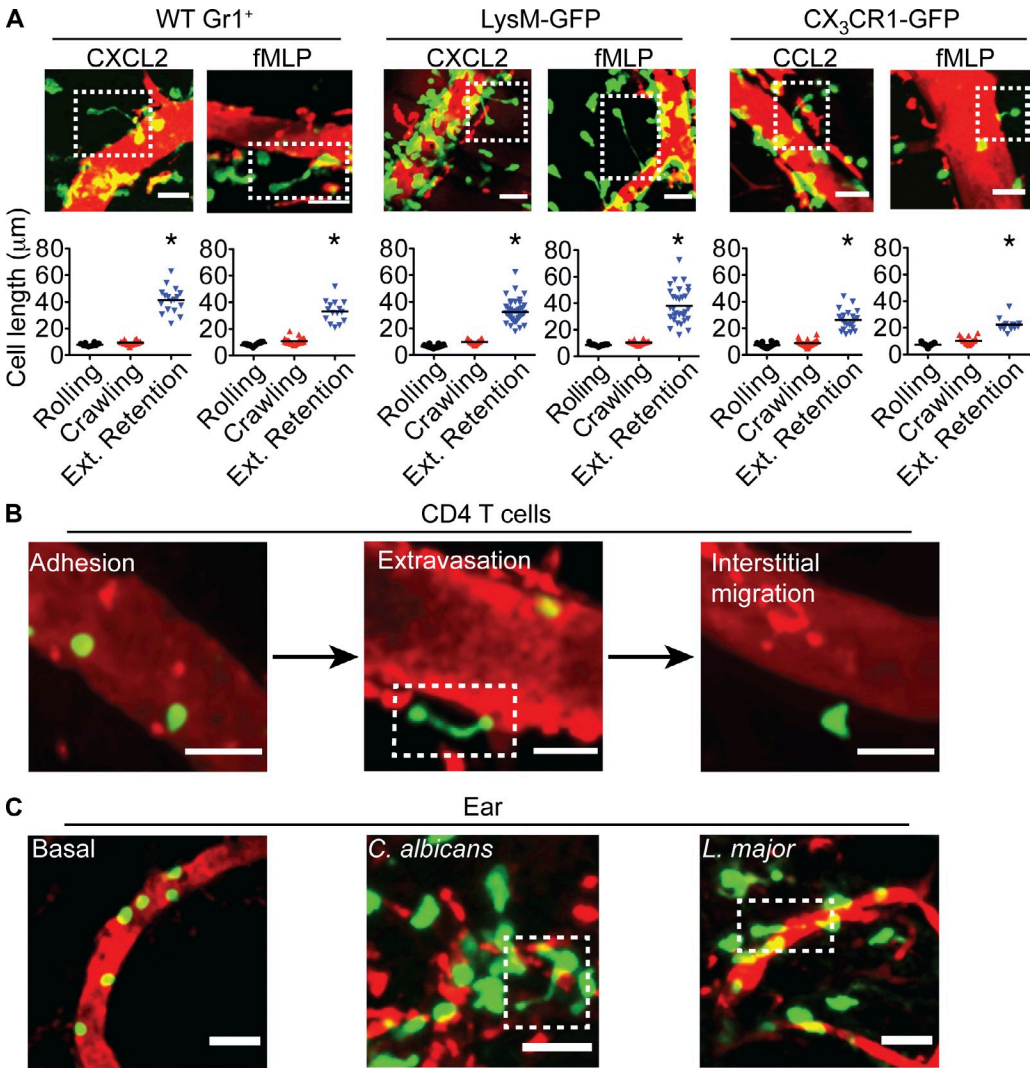

Figure 3. Uropod elongation is a common final step in all leukocyte subsets during extravasation. (A) The cremaster venules in Alexa Fluor 488–anti-Gr1 antibody–injected (i.v.) WT, LysM-GFP, and CX_3CR1-GFP mice were stimulated with chemokines (1 nM CXCL2 or CCL2) and 1 μM fMLP. The representative images of the cell elongation (top) and the cell lengths in each extravasation step (rolling, crawling, and extravascular [Ext.] retention; bottom) are shown. The cell lengths of each extravasating step were measured from at least five stimulated cremaster venules from three mice per stimulatory condition. Horizontal lines indicate the mean. *, $P < 0.005$. See corresponding Videos 2–4. (B) CFSE-labeled effector CD4 T cells were adoptively transferred to the WT recipient mice. The cremaster from the recipient mouse was stimulated with CXCL12 and IP10 and imaged using MP-IVM. The representative images of adhesion, interstitial migration, and elongation of the CD4 T cells are shown in the stimulated cremaster venules of the recipient mice. Cell morphology at each extravasating step was investigated from at least five stimulated cremaster venules from three mice. See corresponding Video 5. (C) MP-IVM was performed on the ear venules of LysM-GFP mice after PBS inoculation (Basal) or infection with *C. albicans* or *L. major*. A representative still image is shown among at least three basal and infected mice ear venule images for each condition. See corresponding Video 6. (A–C) The boxed areas indicate elongated leukocytes. Bars, 30 μm.

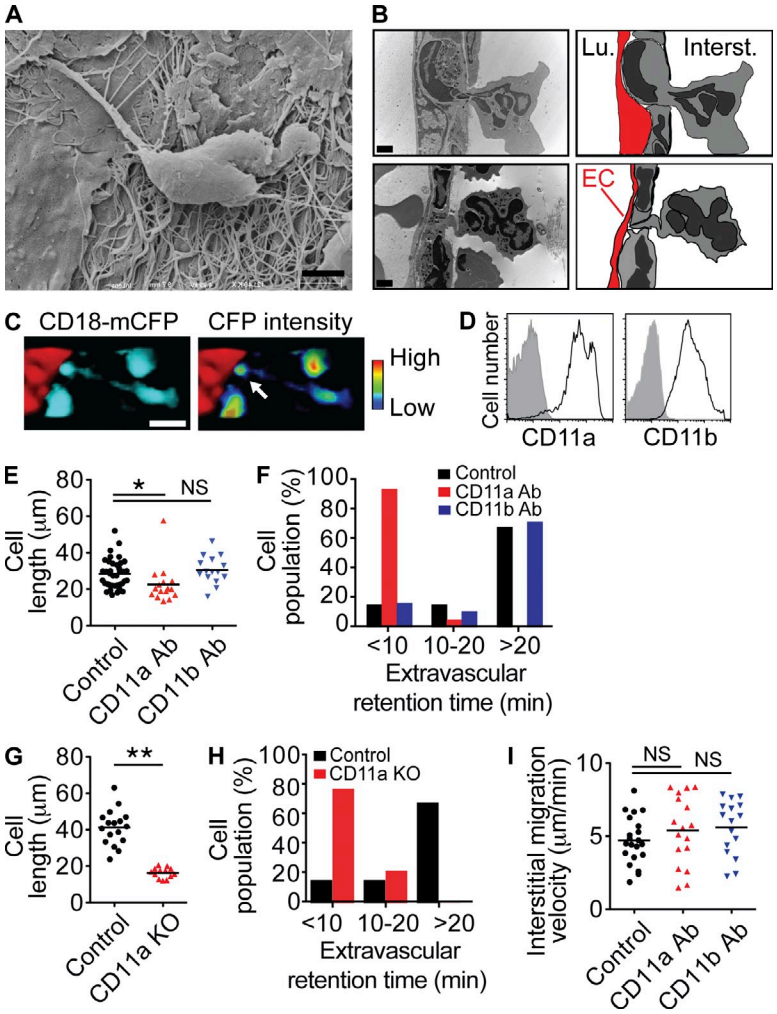

Figure 4. Leukocyte elongation is mediated by LFA-1 at the tail. (A) A scanning EM image of an extravasating leukocyte from the endothelium of a CXCL2-stimulated cremaster from a CD18-mCFP mouse is shown. A representative image is shown from two independent scanning EM experiments. (B) Two representative transmission EM images are shown together with corresponding cartoons that indicate endothelial cells (EC) in red and neutrophils in gray. Among 50 randomly selected neutrophil images from two independent experiments that showed perivascular elongation, 100% of these cells laid the uropod attached to the basolateral side of the endothelial cell layer but not its apical side. Transmission EM was independently performed two times using the CXCL2-stimulated cremasters of CD18-mCFP mice. Interst., interstitium; Lu., lumen. (C) CFP signal in an elongated CD18-mCFP is shown in rainbow colors. Texas red dextran was i.v. injected to indicate the blood vessel (red), the cremaster muscle of CD18-mCFP mice was stimulated with CXCL2, and then the tissue was fixed. The arrow indicates that CD18 is localized at the leukocyte uropod. Three-dimensional images of CFP and Texas red were taken using MP-IVM, and the images were processed as extended images using the Volocity software. Bars: (A and B) 1 µm; (C) 10 µm. (D) Antibody diffusion into the perivascular space through i.v. injection. Mice were immunized in one ear with 5 µg Keyhole Limpet Hemocyanin emulsified in complete Freund's adjuvant. 4 d later, 50 µg PE-conjugated anti–mouse CD11a antibody (M17/4) or CD11b antibody (M1/70) was i.v. injected. After 30 min, the mice were sacrificed, and the leukocytes were extracted from the ear by collagenase digestion of the tissue. In vivo labeling of intradermal leukocytes was then evaluated by flow cytometry. The plot represents the $CD45^+CD4^+$ lymphocytes from anti-CD11a– or anti-CD11b–treated mice (black lines; gray closed histograms indicate PBS-treated mice). (E–H) The cell lengths (E) and extravascular retention times (F) of CD18-mCFP cells were measured in the CXCL2-stimulated cremaster venules of CD18-mCFP mice in the presence of the IgG isotype control or CD11a (M17/4) or CD11b (M1/70) blocking antibodies. The cell lengths (G) and extravascular retention times (H) of the granulocytes labeled with Alexa Fluor 488–anti-Gr1 antibody were measured in WT and CD11a KO mice. The cells were visualized using MP-IVM. The leukocytes located in the interstitium and the intravascular area have been excluded from our analysis. The cell length and the extravascular retention time were measured from images of at least three venules stimulated for >30 min in the cremasters of two CXCL2-stimulated mice. *, $P < 0.05$; **, $P < 0.0001$. See corresponding Videos 7–9. (I) The interstitial migration velocities of CD18-mCFP cells were analyzed in CXCL2-stimulated cremaster tissues from CD18-mCFP mice in the presence of IgG isotype control or CD11a or CD11b blocking antibody using MP-IVM. The velocities were measured from cremaster tissues of two CXCL2-stimulated mice per condition. (E, G, and I) Horizontal lines indicate the mean.

migration can be conceptualized as a cyclic process, where the balance between adhesion at the front and de-adhesion at the rear is important for the regulation of directional cell migration. The velocity profile of extravasating leukocytes showed synchronous movements of the head and tail from intravascular adhesion until completion of TEM (Fig. 5 A and Video 10), suggesting proper balance between adhesion and de-adhesion at the front and rear of migrating cells, respectively. During elongation, however, the speed of the tail was decreased and approached zero as the result of strong LFA-1/ligand binding at the uropod (Fig. 5 A and Video 10). Interestingly, the dramatic inconsistency between the tail and head speeds during cell elongation was not only caused by the decreased tail speed, but also by a two- to threefold increase in the head speed in the near perpendicular direction (angles between 45° and 90°) to the endothelial layer (Fig. 5, A and D; and Video 10). This result suggests the presence of an additional force at the head that can facilitate the penetration of the cells at the leading edge through the basement membrane and their migration into the interstitium.

Although the mechanisms by which leukocytes penetrate the vascular basement membrane are unclear, a blocking antibody against VLA-6 ($\alpha_6\beta_1$) has been shown to inhibit neutrophil crawling along the subendothelial basement membranes (Dangerfield et al., 2002, 2005). However, the involvement of VLA-6 integrin in neutrophil migration is cytokine specific and mediates IL-1β–dependent neutrophil migration in cremaster venules but does not support neutrophil migration in response to TNF or fMLP. Therefore, in this study we focused on another major laminin-binding integrin in neutrophils, VLA-3 ($\alpha_3\beta_1$; CD49c/CD29), which

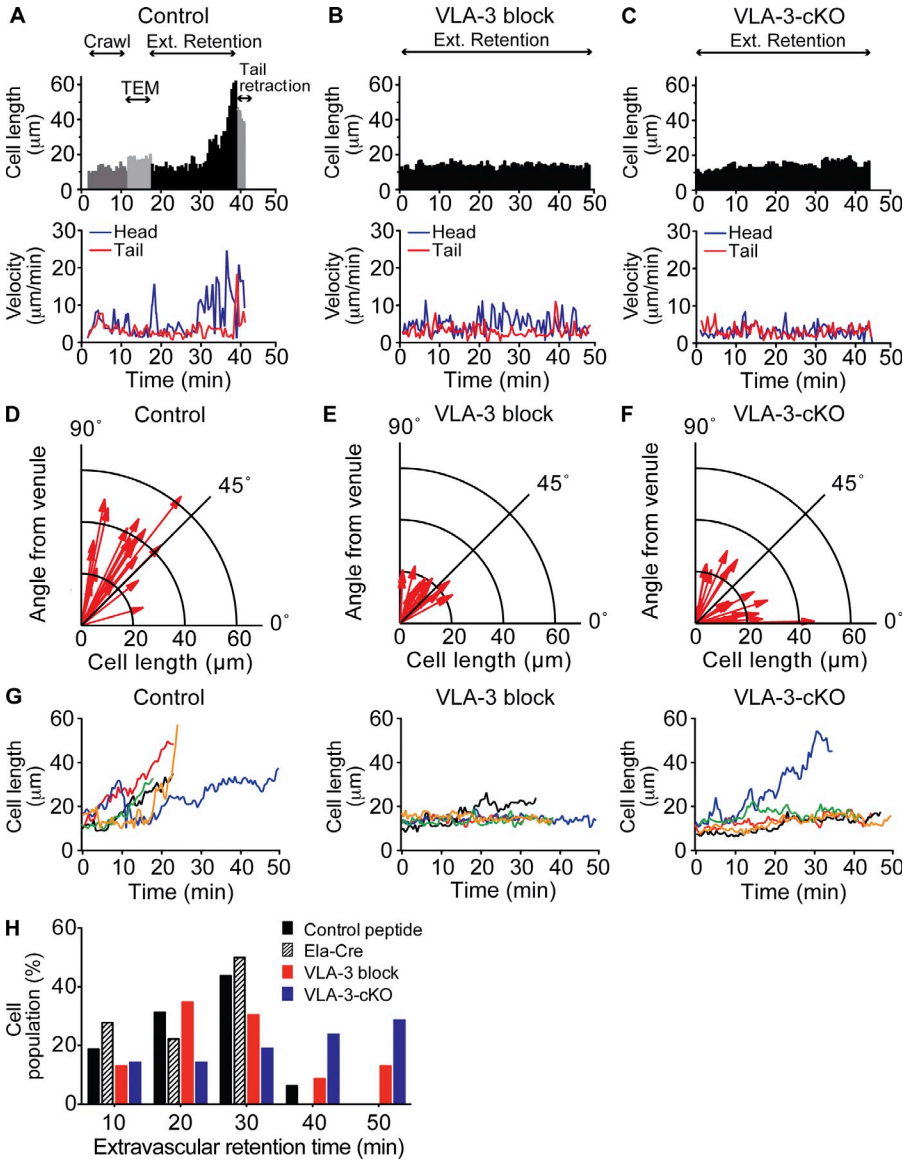

Figure 5. Leukocyte elongation is maintained by VLA-3 integrin–mediated penetration through the endothelial basement membrane at the leading edge. (A–C) The extravasating LysM-GFP cells or Alexa Fluor 488–anti-Gr1 antibody–stained granulocytes were tracked after stimulation with CXCL2 in mice treated with the control (A) or VLA-3 blocking peptide (B) and in VLA-3–cKO mice (C). The cell lengths (top) were measured at each time point during migration. The velocities of the head and tail (bottom) of migrating cells were measured by tracking the positions of the leading edge and uropod at each time point with Volocity software and plotted at the indicated time points. A representative dataset of the cell length and velocity profiles was paired among three independent analyses of each condition. See corresponding Videos 10–12. (D–F) The correlations between the angle from the venule and the cell length during extravasation are shown for control (D), VLA-3 blocking peptide–treated (E), and VLA-3–cKO (F) mice. The cell lengths and the angles from each mouse were analyzed using MP-IVM. The maximum angle of the venule and the longest length of each cell were measured during granulocyte extravasation in MP-IVM. The angles and the cell lengths of extravasating cells were measured from at least five stimulated cremaster venules of three mice. (G) Cell lengths were measured at each time point during extravascular retention in control, VLA-3 blocking peptide–treated, and VLA-3–cKO mice from videos taken with MP-IVM. The data are additional representatives of cell length profiles in A–C. (H) Extravascular retention times were measured in the control peptide treated–, Ela-Cre, VLA-3 blocking peptide–treated, and VLA-3–cKO mice from videos taken with MP-IVM. Extravasating LysM-GFP cells in the cremaster venules of LysM-GFP mice were tracked for the control and VLA-3 blocking peptide treatments. The LXY2 peptide was superfused onto the exteriorized cremaster muscle for VLA-3 integrin blocking. For the analysis of Ela-Cre and VLA-3–cKO mice, Alexa Fluor 488–anti-Gr1 antibody was i.v. injected to visualize the granulocytes. The extravascular retention time was measured from at least five stimulated cremaster venules from three mice per condition.

has been implicated in chemotactic migration on the basement membrane proteins in response to IL8 and fMLP (Yauch et al., 1998; Elphick et al., 2009). In addition to neutrophils, mouse CD4 T cells and monocytes also express high levels of VLA-3 on the cell surface (unpublished data). To assess the function of VLA-3 in leukocyte elongation, the VLA-3 blocking peptide LXY2 was used (Yao et al., 2009). To further determine the precise contributions of VLA-3 during neutrophil extravasation, we generated a conditional KO of VLA-3 (VLA-3–cKO) by crossing α_3-flox mice with those expressing Cre under the granulocyte-specific elastase-2 promoter (Ela-Cre). Deletion of the floxed α_3 subunit allele and absence of the protein were confirmed (not depicted). Blocking VLA-3 with LXY2 completely abolished the increase in the head speed as well as the subsequent elongation of extravasating leukocytes, thus increasing the extravascular retention time (Fig. 5, B, E, G, and H; and Video 11). Importantly, blocking VLA-3 did not decrease cell migration velocity in the tissue interstitium (not depicted; Lämmermann et al., 2008). Compared with control, the VLA-3–cKO neutrophils dramatically inhibited cell elongation and increased the perivascular retention time (Fig. 5, C, F, G, and H; and Video 12). In addition, the VLA-3–cKO neutrophils gained access to the interstitial space using random directions of egress along the entire length of the vessel (Fig. 5 F). Therefore, our data suggest that the uropod elongation during leukocyte extravasation is mediated by a retention force at the contact between the leukocyte uropod and the basolateral

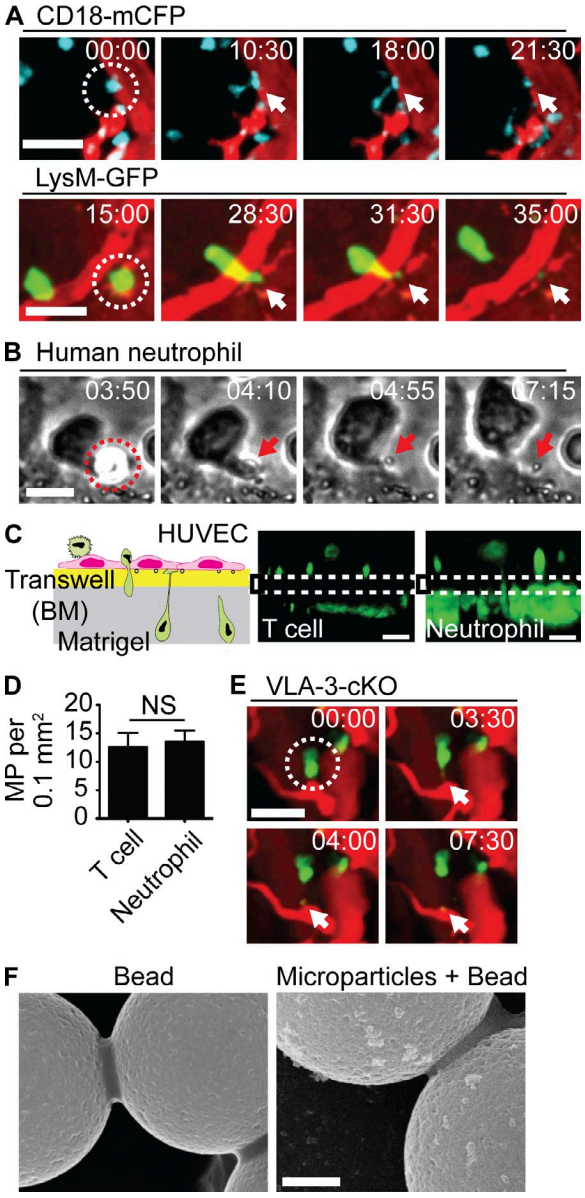

Figure 6. Extravasating leukocytes deposit CD18-enriched microparticles at the subendothelial layer during the stretched uropod retraction. (A) Microparticle formation from the uropods of elongated leukocytes was visualized in the CXCL2-stimulated venules of CD18-mCFP (top) and LysM-GFP mice (bottom). The circles indicate extravasating leukocytes. A series of representative time-lapse images are shown among at least five microparticle formation videos from the MP-IVM analysis of the cremaster venules from CD18-mCFP and LysM-GFP mice. See corresponding Videos 13 and 14. (B) Microparticles were generated from human neutrophils during the in vitro transmigration through a TNF-stimulated HUVEC monolayer. The circle indicates a transmigrating neutrophil through the HUVEC monolayer. A series of representative time-lapse images are shown among three independent microparticle formation videos of in vitro migration. See corresponding Video 15. (A and B) Arrows indicate microparticles. (C) Microparticles formed during the transmigration of primary human T cells and neutrophils toward 0.2 µg chemokines (CXCL12 for T cells and CXCL2 for neutrophils) through a TNF-stimulated HUVEC layer grown on basement membrane (BM)–coated transwells (dashed lines; middle and right). After incubation at 37°C for 1 h, the cells were labeled with anti-CD18 antibodies (CBR LFA1/2 and TS1/18) and Alexa Fluor 488–anti-mouse IgG antibody after fixation. Three-dimensional images were taken using multiphoton microscopy. Representative still images are shown among three microparticle formation videos of the in vitro transwell chemotaxis of human T cells and neutrophils. A schematic description of the assay is shown (left). See corresponding Video 16. (D) Microparticles (MP) derived from transmigrating human T cells and neutrophils were counted. Cell numbers were counted from three independent experiments described in C. The results are expressed as the mean ± SEM. (E) Microparticle formation from the uropods of the elongated granulocytes was visualized in the CXCL2-stimulated venules of VLA-3–cKO mouse by i.v. injection of Alexa Fluor 488–anti-Gr1 antibody. The circle indicates an extravasating leukocyte. The arrow shows the formation of a microparticle. A series of representative time-lapse images are shown from three microparticle formation videos from the MP-IVM analysis of the cremaster venules of VLA-3–cKO mice. See corresponding Video 17. (F) Scanning EM was performed to detect submicrometer-sized LFA-1–expressing microparticles. Microparticles were isolated from CXCL2-stimulated cremaster tissue by collagenase digestion and centrifuge as described in Materials and methods. Magnetic beads conjugated with anti-rat IgG were used to collect CD11a antibody (M17/4)–bound particles from the lower molecular weight fraction than normal cells. Scanning EM of magnetic beads bound to LFA-1–positive particles revealed that there are a large number of LFA-1–expressing microparticles, whose sizes are in submicrometer ranges. Bars: (A and E) 30 µm; (B and C) 10 µm; (F) 1 µm.

membrane of the endothelium, and an additional force at the head, induced by integrins like VLA-3, which interact with components in basement membrane.

Leukocytes deposit microparticles at the endothelium

Consistent with our findings, others also have reported uropod elongation during leukocyte extravasation (Mempel et al., 2003; Peters et al., 2008). However, extreme uropod elongation and prolonged leukocyte extravasation are counterintuitive, as these features might delay the overall immune surveillance and initiation of leukocyte effector functions. We therefore explored the biological consequences of the uropod elongation. Tail elongation and the release of a large fraction of integrin-enriched microparticles from the elongated tail through the damaged cell membrane have been described as a mechanism for uropod detachment during the migration of numerous cell types, including fibroblasts (Regen and Horwitz, 1992; Fuhr et al., 1998; Palecek et al., 1998; Richter et al., 2000; Kirfel et al., 2004; Rigort et al., 2004), cancer cells, T cells, and primary chondrocytes (Zimmermann et al., 2001). MP-IVM analysis of the cremaster venules of CD18-mCFP mice revealed that small microparticles (<1 µm) often remained in the perivascular area, whereas the extravasating leukocytes retracted their tails. These microparticles exhibited CFP intensity, suggesting the presence of CD18 integrins in the particles (Fig. 6 A and Video 13). The generation of microparticles during extravasation was also confirmed using in vivo imaging of LysM-GFP mice (Fig. 6 A and Video 14) and in vitro imaging of human T cells and neutrophils transmigrating through TNF-stimulated human

umbilical vein endothelial cells (HUVECs; Fig. 6, B and C; and Videos 15 and 16). The numbers of microparticles formed from human T cells and neutrophils were not significantly different in our in vitro TEM assay (Fig. 6 D). The microparticles were also readily detected in VLA-3–cKO mice (Fig. 6 E and Video 17), suggesting that the adhesion mediated by LFA-1, but not VLA-3, is more critical for microparticle formation. Indeed, microparticle formation was not observed in CD11a KO mice with MP-IVM (Fig. 4, G and H; and Video 9). To further investigate the presence of leukocyte-derived $CD18^+$ microparticles in the endothelium, we performed scanning EM. After stimulating the mouse cremaster venules with chemokines, the intravascular contents were washed and the venules were digested. The low-molecular-weight fraction, including the submicrometer range of microparticles, was collected using high-speed centrifugation, which has been shown to produce a pure preparation of microparticles (Distler et al., 2005; Scanu et al., 2008; Shefler et al., 2010). The microparticles were subsequently purified using anti–LFA-1 antibody–coated beads. The ultrastructural analysis of the $CD18^+$ microparticles isolated from stimulated tissues showed multiple spherical particles ranging from 100 to 500 nm in diameter (Fig. 6 F). The contractile force at the tail of extravasating leukocytes is important for the retraction of the trailing edge and for squeezing and propelling the cell body through pores in the basement membrane and pericytes (Lämmermann et al., 2008). Members of the nonmuscle myosin II family mediate cellular contraction, and these proteins are controlled by myosin light chain kinase (MLCK) and Rho-associated protein kinases (ROCKs; Morin et al., 2008; Nourshargh et al., 2010). Pretreating cells with blebbistatin or Y27632 (Soriano et al., 2011) resulted in the extreme elongation of tails and the dramatic decrease in transmigration of human T cells and neutrophils through the HUVEC monolayer and the number of microparticles remaining at the basolateral side of HUVECs (unpublished data).

DISCUSSION

Among the established techniques to study leukocyte trafficking in vivo, the direct observation of leukocyte rolling and migration using MP-IVM is one of the most important experimental approaches. Indeed, recent studies of leukocyte trafficking using MP-IVM have provided novel and important insights into the physiological and pathological migration patterns of leukocytes and their role in health and disease. This information has been essential for the development of new antiinflammatory therapies to treat chronic inflammation and autoimmune disease (Lebwohl et al., 2003; Stüve and Bennett, 2007). One of the most common methods for studying distinct leukocyte subsets using MP-IVM involves the isolation and in vitro fluorescent labeling of cells from donor mice followed by their reintroduction into a recipient; however, this approach subjects cells to a large amount of ex vivo handling. Transgenic mice expressing fluorescence proteins in a cell type–specific fashion are alternatives to ex vivo–purified and fluorescently labeled cells. However, transgenic mice only provide information regarding cell shape, tissue distribution, or cell–cell interactions. The goals of this study were to investigate the detailed cellular structure of actively migrating leukocytes at local inflamed tissues and provide knowledge of how leukocytes regulate integrins during the transition from one step to the next in the multistep extravasation cascade. Using newly generated CD18-mCFP KI mice, we have uncovered a final common step in leukocyte extravasation in which the uropods of transmigrating cells remain bound to the endothelium for an extended period of elongation before retracting their tails and migrating into the interstitial tissue space. Second, our experiments have revealed that these cells deposit $CD18^+$ microparticles at the subendothelial layer during extravasation.

LFA-1 and Mac-1 were suggested to have redundant roles during leukocyte migration because in vitro studies reported that both integrins could bind the same ligand (Rothlein et al., 1986; Springer, 1990; Diamond et al., 1991). However, recent intravital imaging studies have shown that LFA-1 and Mac-1 act through distinct mechanisms during leukocyte adhesion and crawling (Phillipson et al., 2006; Shulman et al., 2009). It was suggested that adhesion to the endothelium is mediated by LFA-1, whereas intravascular crawling is mediated by Mac-1 in neutrophils (Phillipson et al., 2006). In monocytes and lymphocytes, however, crawling was shown to be LFA-1 dependent (Auffray et al., 2007; Shulman et al., 2009). This result indicates the possibility that transmigration through the endothelium might be distinctly regulated by LFA-1 and/or Mac-1 in different leukocyte subsets and at different extravasation steps. Our data suggest that the strong interaction between the uropod of leukocytes and the basolateral side of the endothelium during cell elongation is primarily mediated by LFA-1 but not by Mac-1. Consistent with these results, we also observed similar uropod elongation during the in vivo extravasation of effector T cells, which express low levels of Mac-1.

Although there is ample evidence that many leukocyte subsets can generate microparticles and secrete them into the extracellular space (Dalli et al., 2008; Pluskota et al., 2008; Shefler et al., 2010), the function of the leukocyte-derived microparticles is less clear. One of the most important features of microparticles is that they contain cytosolic components of their original cells and expose the extracellular side of the membrane from which they form to the outer surface. Thus, these miniature versions of cells might be an important channel for remote intercellular communications between leukocytes and endothelial cells and other cells within the body. However, it is currently unknown whether all extravasating leukocytes or only a subpopulation of cells are able to generate microparticles because the detection of microparticles (<0.5 μm) has been impeded in our study by the resolution limit of MP-IVM. Alternatively, several mechanisms have been proposed for LFA-1 detachment at the tail during leukocyte migration. In T cells, a contractile force generated by nonmuscle myosin type IIA (MyH9) is critical for detaching inactivated LFA-1 from ICAM-1 and retracting the

uropod (Morin et al., 2008). Evans et al. (2006) has shown in neutrophils and monocytes, but not in lymphocytes, that shedding of an active heterodimeric fragment of LFA-1 plays a role in cell detachment after TEM in cantharidin blister fluid. It was also shown that MMP-9 cleaves between Ala^{705} and Ile^{706} in the CD18 integrins (Vaisar et al., 2009). Thus, it is tempting to speculate that the modulation of LFA-1 deactivation and the detachment from its ligands might control microparticle formation and the extravascular retention time of extravasating leukocytes.

Once leukocytes pass the endothelium, they face another mechanical barrier, the venular basement membrane. It has recently been shown that the venular basement membrane contains preformed regions that express low levels of certain basement membrane components (Wang et al., 2006; Nourshargh et al., 2010). The mechanisms by which leukocytes penetrate the vascular basement membrane structure remain unclear, but depending on the vascular bed and the leukocyte subtype, these mechanisms could involve leukocyte receptors for basement membrane proteins (e.g., integrins) and leukocyte proteases (e.g., neutrophil elastases and MMPs). Indeed, the genetic ablation of VLA-3 and selective inhibition of the VLA-3–laminin interaction significantly decreased neutrophil penetration through the basement membrane and substantially increased the extravascular retention time (Fig. 5). Major ligands for VLA-3 in the basement membrane include laminin-8 ($\alpha4{:}\beta1{:}\gamma1$) and laminin-10 ($\alpha5{:}\beta1{:}\gamma1$). Recruitment of leukocytes was dramatically reduced in laminin-8–deficient mice (Kenne et al., 2010). In addition, the K_d value of VLA-3 for binding to laminin-10 was estimated to be around 1 nM in the presence of Mn^{2+} (Nishiuchi et al., 2003). Therefore, this strongly suggests that, together with VLA-6 (Dangerfield et al., 2002, 2005), VLA-3 may play an important role in guiding leukocytes through the venular basement membrane. VLA-3 is expressed in many human leukocyte subsets as well, including neutrophils (Yauch et al., 1998), monocytes (Ammon et al., 2000), and T cells (Wayner et al., 1993; Sato et al., 1999), with relatively different expression levels. Although comprehensive studies that compare different T cell and monocyte subpopulations or other immune cell types have not been performed, it remains a possibility that these cells use common integrins like VLA-3 during extravasation or the same leukocyte type can use different integrins depending on the local tissue milieus (Dangerfield et al., 2002, 2005).

Previous studies have shown that the LFA-1 interaction with high density ICAM-1 induces leukocyte polarization and migration (Allingham et al., 2007; Dixit et al., 2011; Shulman et al., 2012). Although it is not known whether intracellular signals cross talk between LFA-1 and VLA-3, activated LFA-1 might simultaneously localize at the leading edge along with VLA-3 during early cell adhesion, and the leukocytes might differentially segregate these integrins during extravasation. Nonetheless, in our study, we observed that the majority of the uropod elongations and microparticle formations were mediated through the LFA-1 and ICAM-1 interactions independent of VLA-3–mediated adhesion (Video 17). Thus, we concluded that the basement membrane proteins are not directly involved in the formation of microparticles. Although we cannot completely rule out the possibility that leukocytes interact with ICAM-1–expressing pericytes, our transmission EM data showed that pericytes were rarely present at the site of leukocyte elongation and microparticle formation.

The endothelial lining of the vasculature forms a physical barrier between the blood and the underlying tissues. Therefore, one can assume that disruptions at the endothelial junctions and/or openings in the vascular walls during leukocyte extravasation might cause leakage of fluid and large molecules into the tissues. The direct effect of inflammatory mediators on endothelial cell damage and the contribution of leukocyte extravasation to microvessel permeability are thus easily confounded (He, 2010). However, emerging evidence has shown that cooperative interactions between the endothelium and leukocytes sustain vascular homeostasis during leukocyte TEM under normal immune surveillance and inflammation (Nottebaum et al., 2008; Rowe and Weiss, 2008). The delayed dissociation of the uropods from the subendothelial layer during extravasation might be necessary to provide enough time to reseal the endothelium after TEM; thus, vascular protection could be provided through the generation of $CD18^+$ microparticles from the tip of the uropod. Microparticles likely deposit leukocyte cell membrane on the endothelial cell surface. Therefore, it is tempting to speculate that $CD18^+$ microparticles could function as a membrane seal or represent a special type of paracrine signaling machinery involved in endothelial communications to secure cell–cell junctions. Alternatively, this seal might also act as a guiding structure for trailing or neighboring leukocytes to modulate both the speed and route of their chemotaxis.

MATERIALS AND METHODS

Mice. CD18-mCFP KI mice were generated at the Gene Targeting and Transgenic Core facility at the University of Rochester and backcrossed to C57BL/6 for six generations. For gene targeting, the genomic DNA was isolated from a bacterial artificial chromosome clone containing the mouse integrin CD18 subunit gene. The pBluescript-based target vector, which includes a *loxP* flanked *neo*^{r} cassette, was used. The mCFP gene was fused to the last exon (exon 16) of the CD18 gene with a 6-aa linker (GGPVAT; Kim et al., 2003). The 5′ region of homology, containing exon 16 and the diphtheria toxin (DTA)–negative selection gene, and the 3′ region of homology were subcloned into the up- and downstream regions of the *loxP* flanked *neo*^{r} cassette, respectively. The *neo*^{r} cassette was excised using *Cre* recombinase. For the generation of granulocyte-specific VLA-3 KO mice, Ela-Cre KI mice were purchased from The European Mouse Mutant Archive, in which Cre-recombinase is expressed in the myeloid cells in place of the Ela gene, permitting conditional mutagenesis in the myeloid precursors of target genes tagged with loxP sites (Tkalcevic et al., 2000). Ela-Cre mice were crossed with α_3-Flox (gift from A. Sonnenberg, The Netherlands Cancer Institute, Amsterdam, Netherlands) mice for four to five generations to achieve the deletion of the α_3 gene in the transgenic mice. The mice were genotyped using PCR and DNA isolated from tail tissues. For Ela-Cre, the primers F (5′-CATGACACCCCCACTGTCGTGTCC-3′), R (5′-TGGCACCACAGAAATGACCTCCAC-3′), and Lx (5′-TTTGGTGCACGGTCAGCAGATTGG-3′) were used to generate bands of 615 bp and 185 bp for

WT and mutant, respectively. For the integrin α_3 primers, P1 (5′-GAACA-ACATCTGCCTGGAGT-3′) and P2 (5′-GTATGACTTCTGCCAT-GTAGC-3′) were used to generate bands of 442 bp and 494 bp for WT and flox, respectively. The removal of the gene by Cre-mediated recombination was confirmed using primers P1 and P3 (5′-CAACAGCACT-GCTGTAGCA-3′) to produce a 427-bp band (Margadant et al., 2009). For all experiments and further breeding, the transgenic mice with a brown coat color (coat color of Ela-Cre parents) were selected. VLA-3 expression in VLA-3–cKO, Ela-Cre, and WT mice was detected with polyclonal anti–mouse VLA-3 antibody (AF2787; R&D Systems). C57BL/6, LysM-GFP (Faust et al., 2000), CX_3CR1-GFP (Jung et al., 2000), and CD11a KO (Ding et al., 1999) were maintained in a specific pathogen–free environment at the University of Rochester's animal facility. The Institutional Review Board of the University of Rochester approved all animal experiments.

Mouse neutrophil, T cell, and monocyte preparation. Mouse neutrophils were isolated from bone marrow (Hamada et al., 2009). In brief, femurs and tibias were harvested and stripped of all muscle and sinew. Bone marrow then was flushed out with 10 ml RPMI medium containing 5% FBS on ice. Cells were pelleted by centrifuging for 3 min at 1,500 rpm, and then erythrocytes were depleted. After being resuspended at 5×10^7 cells/ml in HBSS, cells were layered on a Percoll gradient (3 ml of 55%, top; 3 ml of 65%, middle; 4 ml of 80% Percoll) and centrifuged at 2,000 rpm for 30 min at 10°C. Mature neutrophils were finally recovered at the interface of the 65 and 80% fractions. Monocytes were gated with anti-CD115 antibody from bone marrow cells. Naive mouse CD4 T cells were isolated from whole spleen and lymph node suspensions by negative selection using the complement method, purity >80% by flow cytometry. Effector OT-II CD4 T cells were generated through the in vitro activation of naive T cells using the $OVA_{323–339}$ peptide and irradiated T-depleted splenocytes in the presence of 10 U/ml IL-2, 20 ng/ml IL-12, and 40 mg/ml anti–IL-4 (clone 11B11). After 5 days of priming, the effector cells were purified with Ficoll and labeled with CFSE (Invitrogen).

In vitro T cell migration. Delta T dishes (Thermo Fisher Scientific) were coated overnight at 4°C with 20 μg/ml Protein A and 4 μg/ml mouse CCL21 (R&D Systems), washed, and then incubated with 10 μg/ml mouse ICAM-1 (R&D Systems) at room temperature for 2 h. Naive mouse CD4 T cells were placed on the dish. Image acquisition was conducted on a microscope (TE2000-U microscope; Nikon) using 20× objectives coupled to a CoolSNAP HQ charge-coupled device (Roper Scientific). Migration analysis was performed using Volocity software (PerkinElmer).

Adoptive transfer of effector T cells. Effector OT-II CD4 T cells, of which preparation was described in Mouse neutrophil, T cell, and monocyte preparation, were transferred into the recipient mouse immediately before imaging, and the recipient mouse cremaster was superfused with 12.5 nM CXCL12 and 10 nM IP10 (PeproTech) for MP-IVM.

LysM-GFP bone marrow chimeric mice generation. Bone marrow was isolated from both LysM-GFP and C57BL/6 mice. To generate mice with a reduced frequency of LysM-GFP–positive cells, lethally irradiated WT recipients (C57BL/6) received 5×10^6 bone marrow cells/mouse, where 20% and 80% of the cells were derived from LysM-GFP and WT donor mice, respectively. GFP-expressing cells from the peripheral blood were used to confirm the engraftment. 8–12 wk after irradiation, the mice were used for MP-IVM.

MP-IVM of blood vessels in mouse cremaster and ear venules. To visualize leukocyte motility during extravasation, MP-IVM was performed using an FV1000-AOM multiphoton system (Olympus) equipped with a 25× NA1.05 water immersion objective. For two-photon excitation, a Mai-Tai HP Ti:Sa Deep See laser system (Spectra-Physics) was tuned to 820 nm for CFP/Texas red and 900 nm for GFP/Texas red. The images were acquired at a resolution of 256 × 256 pixels, with a pixel dwell time of 2 μs, using step sizes of 1 μm to a depth of 25–30 μm every 30 s. CFP, GFP/CFSE, and Texas red were visualized using band-pass filters with 460/80-nm, 519/25-nm, and 607/26-nm bandwidths, respectively. For imaging the cremaster and ear venules, the mice were initially anesthetized through an intraperitoneal injection of pentobarbital sodium at a dose of 65 mg/kg, and the hair on the skin of the imaging area was removed. For imaging the cremaster blood vessels, the right cremaster muscle was exteriorized and covered with warmed physiological solution (containing the following components: 131.9 mM NaCl, 4.7 mM KCl, 2.0 mM $CaCl_2$, 1.2 mM $MgSO_4$, and 18 mM $NaHCO_3$, pH 7.4) at 37°C and equilibrated with gas containing 0% O_2, 5% CO_2, and 95% N_2 to maintain tissue PO_2 <15 torr (Kim and Sarelius, 2004). The mice were subsequently placed on a custom-designed platform, and anesthesia was maintained with isoflurane for restraint and to avoid psychological stress and pain on the animal during imaging. The core body temperature of the mice was maintained using a warming pad set to 37°C, and Texas red dextran (70,000 molecular weight; Invitrogen) was i.v. injected (20 mg/kg) via femoral vein to label the blood vessels immediately before imaging. To image granulocytes in WT, CD11a KO, Ela-Cre, or VLA-3–cKO mice, 0.12 mg/kg Alexa Fluor 488–anti-Gr1 antibody was i.v. injected during experiments. The blood vessels were stimulated by superfusion of chemokines (1 nM CXCL2 or CCL2) or the bacterial chemoattractant (1 μM fMLP). For TNF stimulation, TNF (0.5 μg in 250 μl saline) was intrascrotally injected 4 h before in vivo imaging. To investigate the effect of CD18 integrin inhibition on leukocyte extravasation, 100 μg CD11a (M17/4) or CD11b (M1/70) blocking antibody was i.v. injected in the presence of CXCL2. To investigate the role for VLA-3 integrin on leukocyte extravasation, 100 nM VLA-3 blocking peptide was superfused, or VLA-3–cKO was used. For imaging the infected ears, *C. albicans* (from M. Wellington, University of Rochester Medical Center, Rochester, NY) or *L. major* in 10 μl PBS buffer (10^5 cells/ear) was intradermally injected into LysM-GFP mice 6 h before in vivo imaging. The anesthetized mice were laid in a lateral recumbent position on a custom-designed platform to expose the ventral side of the ear pinna for imaging. For observations of extravasating leukocytes, venules with diameter range 20–60 μm were chosen. For interstitial migration of leukocytes, the interstitium was randomly selected 20 μm outside vessels. Volocity software was used to track the morphological changes and movements of the leukocytes.

EM. Leukocyte extravasation was first observed in the CXCL2-stimulated cremaster venules of CD18-mCFP mice using MP-IVM. The cremaster was immediately dissected from the body after euthanization and fixed with 2.5% glutaraldehyde. The tissue was further processed for scanning and transmission EM in the Electron Microscope Research Core at the University of Rochester.

HUVEC-grown transwell migration of human T cells and neutrophils. HUVECs were grown on basement membrane protein–coated transwells and stimulated with TNF. T cells and neutrophils were prepared from human PBMCs. In brief, HUVECs were grown to confluency in transwells coated with the basement membrane extract (Corning) overnight before being placed on Matrigel (BD) prepared with 0.2 μg chemokines (CXCL12 for T cells; CXCL2 for neutrophils) in a 24-well plate. After the HUVECs were stimulated with TNF (0.1 μg per transwell insert) at 37°C for 4 h, 10^5 T cells or neutrophils were placed in the transwell and incubated at 37°C for 1 h. The cells were fixed, and then the transwell was carefully separated. Multiphoton or confocal microscopy was used to obtain three-dimensional images of the transwell for detection of leukocytes and microparticles.

Microparticle characterization with scanning EM. The cremaster muscles of C57BL/6 mice were superfused with saline solution containing CXCL12 at 37°C for 2 h. After euthanasia, the blood was immediately washed out with 10 ml PBS buffer, and then the cremaster muscle was minced. The minced tissue was treated with 3 ml of 0.5% Collagenase II (Invitrogen) in HBSS containing 3 mM $CaCl_2$ at 37°C for 1 h. The supernatant was collected after high-speed centrifugation and then labeled with anti–mouse

CD11a antibody (M17/4). Then the microparticles in 1 ml PBS buffer were incubated with 50 µl Dynabeads sheep anti–rat IgG (Invitrogen) at 4°C for 20 min. The incubated microparticles with Dynabeads were applied to the Dynal magnet for bead-bound particle separation. The microparticles were then further processed for scanning EM as described above.

Statistics. Statistical significance ($P < 0.05$) was computed with the Kruskal–Wallis test or Student's *t* test using Prism software (GraphPad Software).

Online supplemental material. Video 1 shows that leukocytes in CD18-mCFP KI mice were firmly adhered to the intravascular lumen and then extremely elongated during extravasation after stimulation with CXCL2 or TNF. Videos 2–5 show the uropod elongation during extravasation of $Gr1^+$ granulocytes, LysM-GFP^+ cells, CX_3CR1-GFP^+ monocytes, and effector CD4 T cells. Video 6 shows the uropod elongation of LysM-GFP^+ cell extravasation through the infected mouse ear venules. Videos 7 and 8 show the effect of i.v. injected Mac-1 and LFA-1 blocking antibodies on the uropod elongation. Video 9 shows that the uropod elongation and the extravascular retention time in CD11a KO mice are reduced during leukocyte extravasation. Video 10 shows each step of leukocyte extravasation cascade in LysM-GFP mice. Videos 11 and 12 show the effects of VLA-3 blocking with LXY2 peptide and genetic ablation of VLA-3 on leukocyte extravasation. Videos 13 and 14 show microparticle formation from an extravasating leukocyte in CD18-mCFP and LysM-GFP mice. Video 15 shows microparticle formation from a transmigrating human neutrophil through a HUVEC monolayer in vitro. Video 16 shows microparticle formation from human T cell and neutrophil transmigration through a HUVEC monolayer grown on transwells. Video 17 shows microparticle formation from extravasating neutrophils in VLA-3–cKO mice. Online supplemental material is available at http://www.jem.org/cgi/content/full/jem.20111426/DC1.

We thank Melanie Wellington for providing *C. albicans*. We thank Lin Gan, Karl A. Kasischke, and Hung-Li Chung for their technical assistance and Tara Capece for comments on the manuscript.

This project was financially supported through grants from the National Institutes of Health (HL087088 and HL018208 to M. Kim) and the American Heart Association (11SDG7520018 to Y.-M. Hyun).

The authors have no conflicting financial interests.

Author contributions: Y.-M. Hyun designed and performed experiments and analyzed data. R. Sumagin contributed to the intravital imaging and in vivo analysis of rolling and adhering leukocytes. E. Lomakina performed the human neutrophil transmigration in the HUVEC monolayer. P.P. Sarangi conducted the bacterial clearance assay and generated VLA-3–cKO mice. M.G. Overstreet generated LysM-GFP–mixed bone marrow chimeric mice and prepared effector CD4 T cells. C.M. Baker prepared effector CD4 T cells. D.J. Fowell, R.E. Waugh, and I.H. Sarelius designed research and analyzed data. M. Kim conceived, designed, and directed the study. Y.-M. Hyun and M. Kim wrote the manuscript.

Submitted: 12 July 2011
Accepted: 30 May 2012

REFERENCES

Allingham, M.J., J.D. van Buul, and K. Burridge. 2007. ICAM-1-mediated, Src- and Pyk2-dependent vascular endothelial cadherin tyrosine phosphorylation is required for leukocyte transendothelial migration. *J. Immunol.* 179:4053–4064.

Ammon, C., S.P. Meyer, L. Schwarzfischer, S.W. Krause, R. Andreesen, and M. Kreutz. 2000. Comparative analysis of integrin expression on monocyte-derived macrophages and monocyte-derived dendritic cells. *Immunology*. 100:364–369. http://dx.doi.org/10.1046/j.1365-2567.2000.00056.x

Auffray, C., D. Fogg, M. Garfa, G. Elain, O. Join-Lambert, S. Kayal, S. Sarnacki, A. Cumano, G. Lauvau, and F. Geissmann. 2007. Monitoring of blood vessels and tissues by a population of monocytes with patrolling behavior. *Science*. 317:666–670. http://dx.doi.org/10.1126/science.1142883

Bartholomäus, I., N. Kawakami, F. Odoardi, C. Schläger, D. Miljkovic, J.W. Ellwart, W.E. Klinkert, C. Flügel-Koch, T.B. Issekutz, H. Wekerle, and A. Flügel. 2009. Effector T cell interactions with meningeal vascular structures in nascent autoimmune CNS lesions. *Nature*. 462:94–98. http://dx.doi.org/10.1038/nature08478

Bonasio, R., C.V. Carman, E. Kim, P.T. Sage, K.R. Love, T.R. Mempel, T.A. Springer, and U.H. von Andrian. 2007. Specific and covalent labeling of a membrane protein with organic fluorochromes and quantum dots. *Proc. Natl. Acad. Sci. USA*. 104:14753–14758. http://dx.doi.org/10.1073/pnas.0705201104

Burns, A.R., D.C. Walker, E.S. Brown, L.T. Thurmon, R.A. Bowden, C.R. Keese, S.I. Simon, M.L. Entman, and C.W. Smith. 1997. Neutrophil transendothelial migration is independent of tight junctions and occurs preferentially at tricellular corners. *J. Immunol.* 159:2893–2903.

Carman, C.V., and T.A. Springer. 2004. A transmigratory cup in leukocyte diapedesis both through individual vascular endothelial cells and between them. *J. Cell Biol.* 167:377–388. http://dx.doi.org/10.1083/jcb.200404129

Chiang, E.Y., A. Hidalgo, J. Chang, and P.S. Frenette. 2007. Imaging receptor microdomains on leukocyte subsets in live mice. *Nat. Methods*. 4:219–222. http://dx.doi.org/10.1038/nmeth1018

Dalli, J., L.V. Norling, D. Renshaw, D. Cooper, K.Y. Leung, and M. Perretti. 2008. Annexin 1 mediates the rapid anti-inflammatory effects of neutrophil-derived microparticles. *Blood*. 112:2512–2519. http://dx.doi.org/10.1182/blood-2008-02-140533

Dangerfield, J., K.Y. Larbi, M.T. Huang, A. Dewar, and S. Nourshargh. 2002. PECAM-1 (CD31) homophilic interaction up-regulates $\alpha_6\beta_1$ on transmigrated neutrophils in vivo and plays a functional role in the ability of α_6 integrins to mediate leukocyte migration through the perivascular basement membrane. *J. Exp. Med.* 196:1201–1211. http://dx.doi.org/10.1084/jem.20020324

Dangerfield, J.P., S. Wang, and S. Nourshargh. 2005. Blockade of alpha6 integrin inhibits IL-1beta- but not TNF-alpha-induced neutrophil transmigration in vivo. *J. Leukoc. Biol.* 77:159–165. http://dx.doi.org/10.1189/jlb.0704421

Diamond, M.S., D.E. Staunton, S.D. Marlin, and T.A. Springer. 1991. Binding of the integrin Mac-1 (CD11b/CD18) to the third immunoglobulin-like domain of ICAM-1 (CD54) and its regulation by glycosylation. *Cell*. 65:961–971. http://dx.doi.org/10.1016/0092-8674(91)90548-D

Ding, Z.M., J.E. Babensee, S.I. Simon, H. Lu, J.L. Perrard, D.C. Bullard, X.Y. Dai, S.K. Bromley, M.L. Dustin, M.L. Entman, et al. 1999. Relative contribution of LFA-1 and Mac-1 to neutrophil adhesion and migration. *J. Immunol.* 163:5029–5038.

Distler, J.H., A. Jüngel, L.C. Huber, C.A. Seemayer, C.F. Reich III, R.E. Gay, B.A. Michel, A. Fontana, S. Gay, D.S. Pisetsky, and O. Distler. 2005. The induction of matrix metalloproteinase and cytokine expression in synovial fibroblasts stimulated with immune cell microparticles. *Proc. Natl. Acad. Sci. USA*. 102:2892–2897. http://dx.doi.org/10.1073/pnas.0409781102

Dixit, N., I. Yamayoshi, A. Nazarian, and S.I. Simon. 2011. Migrational guidance of neutrophils is mechanotransduced via high-affinity LFA-1 and calcium flux. *J. Immunol.* 187:472–481. http://dx.doi.org/10.4049/jimmunol.1004197

Elphick, G.F., P.P. Sarangi, Y.M. Hyun, J.A. Hollenbaugh, A. Ayala, W.L. Biffl, H.L. Chung, A.R. Rezaie, J.L. McGrath, D.J. Topham, et al. 2009. Recombinant human activated protein C inhibits integrin-mediated neutrophil migration. *Blood*. 113:4078–4085. http://dx.doi.org/10.1182/blood-2008-09-180968

Evans, B.J., A. McDowall, P.C. Taylor, N. Hogg, D.O. Haskard, and R.C. Landis. 2006. Shedding of lymphocyte function-associated antigen-1 (LFA-1) in a human inflammatory response. *Blood*. 107:3593–3599. http://dx.doi.org/10.1182/blood-2005-09-3695

Faust, N., F. Varas, L.M. Kelly, S. Heck, and T. Graf. 2000. Insertion of enhanced green fluorescent protein into the lysozyme gene creates mice with green fluorescent granulocytes and macrophages. *Blood*. 96:719–726.

Friedman, R.S., P. Beemiller, C.M. Sorensen, J. Jacobelli, and M.F. Krummel. 2010. Real-time analysis of T cell receptors in naive cells in vitro

and in vivo reveals flexibility in synapse and signaling dynamics. *J. Exp. Med.* 207:2733–2749. http://dx.doi.org/10.1084/jem.20091201

Fuhr, G., E. Richter, H. Zimmermann, H. Hitzler, H. Niehus, and R. Hagedorn. 1998. Cell traces—footprints of individual cells during locomotion and adhesion. *Biol. Chem.* 379:1161–1173. http://dx.doi.org/10.1515/bchm.1998.379.8-9.1161

Hamada, T., S. Duarte, S. Tsuchihashi, R.W. Busuttil, and A.J. Coito. 2009. Inducible nitric oxide synthase deficiency impairs matrix metalloproteinase-9 activity and disrupts leukocyte migration in hepatic ischemia/reperfusion injury. *Am. J. Pathol.* 174:2265–2277. http://dx.doi.org/10.2353/ajpath.2009.080872

He, P. 2010. Leucocyte/endothelium interactions and microvessel permeability: coupled or uncoupled? *Cardiovasc. Res.* 87:281–290. http://dx.doi.org/10.1093/cvr/cvq140

Huang, A.J., M.B. Furie, S.C. Nicholson, J. Fischbarg, L.S. Liebovitch, and S.C. Silverstein. 1988. Effects of human neutrophil chemotaxis across human endothelial cell monolayers on the permeability of these monolayers to ions and macromolecules. *J. Cell. Physiol.* 135:355–366. http://dx.doi.org/10.1002/jcp.1041350302

Jung, S., J. Aliberti, P. Graemmel, M.J. Sunshine, G.W. Kreutzberg, A. Sher, and D.R. Littman. 2000. Analysis of fractalkine receptor CX(3)CR1 function by targeted deletion and green fluorescent protein reporter gene insertion. *Mol. Cell. Biol.* 20:4106–4114. http://dx.doi.org/10.1128/MCB.20.11.4106-4114.2000

Kenne, E., O. Soehnlein, G. Genové, P. Rotzius, E.E. Eriksson, and L. Lindbom. 2010. Immune cell recruitment to inflammatory loci is impaired in mice deficient in basement membrane protein laminin alpha4. *J. Leukoc. Biol.* 88:523–528.

Kim, M.B., and I.H. Sarelius. 2004. Role of shear forces and adhesion molecule distribution on P-selectin-mediated leukocyte rolling in postcapillary venules. *Am. J. Physiol. Heart Circ. Physiol.* 287:H2705–H2711. http://dx.doi.org/10.1152/ajpheart.00448.2004

Kim, M., C.V. Carman, and T.A. Springer. 2003. Bidirectional transmembrane signaling by cytoplasmic domain separation in integrins. *Science.* 301:1720–1725. http://dx.doi.org/10.1126/science.1084174

Kirfel, G., A. Rigort, B. Borm, and V. Herzog. 2004. Cell migration: mechanisms of rear detachment and the formation of migration tracks. *Eur. J. Cell Biol.* 83:717–724. http://dx.doi.org/10.1078/0171-9335-00421

Lämmermann, T., B.L. Bader, S.J. Monkley, T. Worbs, R. Wedlich-Söldner, K. Hirsch, M. Keller, R. Förster, D.R. Critchley, R. Fässler, and M. Sixt. 2008. Rapid leukocyte migration by integrin-independent flowing and squeezing. *Nature.* 453:51–55. http://dx.doi.org/10.1038/nature06887

Lebwohl, M., S.K. Tyring, T.K. Hamilton, D. Toth, S. Glazer, N.H. Tawfik, P. Walicke, W. Dummer, X. Wang, M.R. Garovoy, and D. Pariser; Efalizumab Study Group. 2003. A novel targeted T-cell modulator, efalizumab, for plaque psoriasis. *N. Engl. J. Med.* 349:2004–2013. http://dx.doi.org/10.1056/NEJMoa030002

Margadant, C., K. Raymond, M. Kreft, N. Sachs, H. Janssen, and A. Sonnenberg. 2009. Integrin alpha3beta1 inhibits directional migration and wound re-epithelialization in the skin. *J. Cell Sci.* 122:278–288. http://dx.doi.org/10.1242/jcs.029108

Mempel, T.R., C. Moser, J. Hutter, W.M. Kuebler, and F. Krombach. 2003. Visualization of leukocyte transendothelial and interstitial migration using reflected light oblique transillumination in intravital video microscopy. *J. Vasc. Res.* 40:435–441. http://dx.doi.org/10.1159/000073902

Morin, N.A., P.W. Oakes, Y.M. Hyun, D. Lee, Y.E. Chin, M.R. King, T.A. Springer, M. Shimaoka, J.X. Tang, J.S. Reichner, and M. Kim. 2008. Nonmuscle myosin heavy chain IIA mediates integrin LFA-1 deadhesion during T lymphocyte migration. *J. Exp. Med.* 205:195–205. (published erratum appears in *J. Exp. Med.* 2008. 205:993) http://dx.doi.org/10.1084/jem.20071543

Nishiuchi, R., O. Murayama, H. Fujiwara, J. Gu, T. Kawakami, S. Aimoto, Y. Wada, and K. Sekiguchi. 2003. Characterization of the ligand-binding specificities of integrin alpha3beta1 and alpha6beta1 using a panel of purified laminin isoforms containing distinct alpha chains. *J. Biochem.* 134:497–504. http://dx.doi.org/10.1093/jb/mvg185

Nottebaum, A.F., G. Cagna, M. Winderlich, A.C. Gamp, R. Linnepe, C. Polaschegg, K. Filippova, R. Lyck, B. Engelhardt, O. Kamenyeva, et al. 2008. VE-PTP maintains the endothelial barrier via plakoglobin and becomes dissociated from VE-cadherin by leukocytes and by VEGF. *J. Exp. Med.* 205:2929–2945. http://dx.doi.org/10.1084/jem.20080406

Nourshargh, S., P.L. Hordijk, and M. Sixt. 2010. Breaching multiple barriers: leukocyte motility through venular walls and the interstitium. *Nat. Rev. Mol. Cell Biol.* 11:366–378. http://dx.doi.org/10.1038/nrm2889

Palecek, S.P., A. Huttenlocher, A.F. Horwitz, and D.A. Lauffenburger. 1998. Physical and biochemical regulation of integrin release during rear detachment of migrating cells. *J. Cell Sci.* 111:929–940.

Peters, N.C., J.G. Egen, N. Secundino, A. Debrabant, N. Kimblin, S. Kamhawi, P. Lawyer, M.P. Fay, R.N. Germain, and D. Sacks. 2008. In vivo imaging reveals an essential role for neutrophils in leishmaniasis transmitted by sand flies. *Science.* 321:970–974. http://dx.doi.org/10.1126/science.1159194

Phillipson, M., B. Heit, P. Colarusso, L. Liu, C.M. Ballantyne, and P. Kubes. 2006. Intraluminal crawling of neutrophils to emigration sites: a molecularly distinct process from adhesion in the recruitment cascade. *J. Exp. Med.* 203:2569–2575. http://dx.doi.org/10.1084/jem.20060925

Phillipson, M., J. Kaur, P. Colarusso, C.M. Ballantyne, and P. Kubes. 2008. Endothelial domes encapsulate adherent neutrophils and minimize increases in vascular permeability in paracellular and transcellular emigration. *PLoS ONE.* 3:e1649. http://dx.doi.org/10.1371/journal.pone.0001649

Pluskota, E., N.M. Woody, D. Szpak, C.M. Ballantyne, D.A. Soloviev, D.I. Simon, and E.F. Plow. 2008. Expression, activation, and function of integrin alphaMbeta2 (Mac-1) on neutrophil-derived microparticles. *Blood.* 112:2327–2335. http://dx.doi.org/10.1182/blood-2007-12-127183

Regen, C.M., and A.F. Horwitz. 1992. Dynamics of beta 1 integrin-mediated adhesive contacts in motile fibroblasts. *J. Cell Biol.* 119:1347–1359. http://dx.doi.org/10.1083/jcb.119.5.1347

Richter, E., H. Hitzler, H. Zimmermann, R. Hagedorn, and G. Fuhr. 2000. Trace formation during locomotion of L929 mouse fibroblasts continuously recorded by interference reflection microscopy (IRM). *Cell Motil. Cytoskeleton.* 47:38–47. http://dx.doi.org/10.1002/1097-0169(200009)47:1<38::AID-CM4>3.0.CO;2-W

Rigort, A., J. Grünewald, V. Herzog, and G. Kirfel. 2004. Release of integrin macroaggregates as a mechanism of rear detachment during keratinocyte migration. *Eur. J. Cell Biol.* 83:725–733. http://dx.doi.org/10.1078/0171-9335-00431

Rittirsch, D., M.S. Huber-Lang, M.A. Flierl, and P.A. Ward. 2009. Immunodesign of experimental sepsis by cecal ligation and puncture. *Nat. Protoc.* 4:31–36. http://dx.doi.org/10.1038/nprot.2008.214

Rothlein, R., M.L. Dustin, S.D. Marlin, and T.A. Springer. 1986. A human intercellular adhesion molecule (ICAM-1) distinct from LFA-1. *J. Immunol.* 137:1270–1274.

Rowe, R.G., and S.J. Weiss. 2008. Breaching the basement membrane: who, when and how? *Trends Cell Biol.* 18:560–574. http://dx.doi.org/10.1016/j.tcb.2008.08.007

Sarantos, M.R., H. Zhang, U.Y. Schaff, N. Dixit, H.N. Hayenga, C.A. Lowell, and S.I. Simon. 2008. Transmigration of neutrophils across inflamed endothelium is signaled through LFA-1 and Src family kinase. *J. Immunol.* 181:8660–8669.

Sato, K., K. Katagiri, S. Hattori, T. Tsuji, T. Irimura, S. Irie, and T. Katagiri. 1999. Laminin 5 promotes activation and apoptosis of the T cells expressing alpha3beta1 integrin. *Exp. Cell Res.* 247:451–460. http://dx.doi.org/10.1006/excr.1998.4374

Scanu, A., N. Molnarfi, K.J. Brandt, L. Gruaz, J.M. Dayer, and D. Burger. 2008. Stimulated T cells generate microparticles, which mimic cellular contact activation of human monocytes: differential regulation of pro- and anti-inflammatory cytokine production by high-density lipoproteins. *J. Leukoc. Biol.* 83:921–927. http://dx.doi.org/10.1189/jlb.0807551

Shaw, S.K., S. Ma, M.B. Kim, R.M. Rao, C.U. Hartman, R.M. Froio, L. Yang, T. Jones, Y. Liu, A. Nusrat, et al. 2004. Coordinated redistribution of leukocyte LFA-1 and endothelial cell ICAM-1 accompany neutrophil transmigration. *J. Exp. Med.* 200:1571–1580. http://dx.doi.org/10.1084/jem.20040965

Shefler, I., P. Salamon, T. Reshef, A. Mor, and Y.A. Mekori. 2010. T cell-induced mast cell activation: a role for microparticles released from activated T cells. *J. Immunol.* 185:4206–4212. http://dx.doi.org/10.4049/jimmunol.1000409

Shulman, Z., V. Shinder, E. Klein, V. Grabovsky, O. Yeger, E. Geron, A. Montresor, M. Bolomini-Vittori, S.W. Feigelson, T. Kirchhausen, et al. 2009. Lymphocyte crawling and transendothelial migration require chemokine triggering of high-affinity LFA-1 integrin. *Immunity.* 30:384–396. http://dx.doi.org/10.1016/j.immuni.2008.12.020

Shulman, Z., S.J. Cohen, B. Roediger, V. Kalchenko, R. Jain, V. Grabovsky, E. Klein, V. Shinder, L. Stoler-Barak, S.W. Feigelson, et al. 2012. Transendothelial migration of lymphocytes mediated by intraendothelial vesicle stores rather than by extracellular chemokine depots. *Nat. Immunol.* 13:67–76. http://dx.doi.org/10.1038/ni.2173

Soriano, S.F., M. Hons, K. Schumann, V. Kumar, T.J. Dennier, R. Lyck, M. Sixt, and J.V. Stein. 2011. In vivo analysis of uropod function during physiological T cell trafficking. *J. Immunol.* 187:2356–2364. http://dx.doi.org/10.4049/jimmunol.1100935

Springer, T.A. 1990. Adhesion receptors of the immune system. *Nature.* 346:425–434. http://dx.doi.org/10.1038/346425a0

Stüve, O., and J.L. Bennett. 2007. Pharmacological properties, toxicology and scientific rationale for the use of natalizumab (Tysabri) in inflammatory diseases. *CNS Drug Rev.* 13:79–95. http://dx.doi.org/10.1111/j.1527-3458.2007.00003.x

Sumagin, R., H. Prizant, E. Lomakina, R.E. Waugh, and I.H. Sarelius. 2010. LFA-1 and Mac-1 define characteristically different intralumenal crawling and emigration patterns for monocytes and neutrophils in situ. *J. Immunol.* 185:7057–7066. http://dx.doi.org/10.4049/jimmunol.1001638

Tkalcevic, J., M. Novelli, M. Phylactides, J.P. Iredale, A.W. Segal, and J. Roes. 2000. Impaired immunity and enhanced resistance to endotoxin in the absence of neutrophil elastase and cathepsin G. *Immunity.* 12:201–210. http://dx.doi.org/10.1016/S1074-7613(00)80173-9

Vaisar, T., S.Y. Kassim, I.G. Gomez, P.S. Green, S. Hargarten, P.J. Gough, W.C. Parks, C.L. Wilson, E.W. Raines, and J.W. Heinecke. 2009. MMP-9 sheds the beta2 integrin subunit (CD18) from macrophages. *Mol. Cell. Proteomics.* 8:1044–1060. http://dx.doi.org/10.1074/mcp.M800449-MCP200

von Andrian, U.H., and C.R. Mackay. 2000. T-cell function and migration. Two sides of the same coin. *N. Engl. J. Med.* 343:1020–1034. http://dx.doi.org/10.1056/NEJM200010053431407

Wang, S., M.B. Voisin, K.Y. Larbi, J. Dangerfield, C. Scheiermann, M. Tran, P.H. Maxwell, L. Sorokin, and S. Nourshargh. 2006. Venular basement membranes contain specific matrix protein low expression regions that act as exit points for emigrating neutrophils. *J. Exp. Med.* 203:1519–1532. http://dx.doi.org/10.1084/jem.20051210

Wayner, E.A., S.G. Gil, G.F. Murphy, M.S. Wilke, and W.G. Carter. 1993. Epiligrin, a component of epithelial basement membranes, is an adhesive ligand for alpha 3 beta 1 positive T lymphocytes. *J. Cell Biol.* 121:1141–1152. http://dx.doi.org/10.1083/jcb.121.5.1141

Yao, N., W. Xiao, X. Wang, J. Marik, S.H. Park, Y. Takada, and K.S. Lam. 2009. Discovery of targeting ligands for breast cancer cells using the one-bead one-compound combinatorial method. *J. Med. Chem.* 52:126–133. http://dx.doi.org/10.1021/jm801062d

Yauch, R.L., F. Berditchevski, M.B. Harler, J. Reichner, and M.E. Hemler. 1998. Highly stoichiometric, stable, and specific association of integrin alpha3beta1 with CD151 provides a major link to phosphatidylinositol 4-kinase, and may regulate cell migration. *Mol. Biol. Cell.* 9:2751–2765.

Zeng, M., H. Zhang, C. Lowell, and P. He. 2002. Tumor necrosis factor-alpha-induced leukocyte adhesion and microvessel permeability. *Am. J. Physiol. Heart Circ. Physiol.* 283:H2420–H2430.

Zimmermann, U., F. Thürmer, A. Jork, M. Weber, S. Mimietz, M. Hillgärtner, F. Brunnenmeier, H. Zimmermann, I. Westphal, G. Fuhr, et al. 2001. A novel class of amitogenic alginate microcapsules for long-term immunoisolated transplantation. *Ann. N. Y. Acad. Sci.* 944:199–215. http://dx.doi.org/10.1111/j.1749-6632.2001.tb03833.x